

# Numerical Finite Element Analysis of the Soil Mass Subjected to the Impulsive Load of a Standard Penetration Test (SPT): Assessment of Young's Modulus of Soils

Zoa Ambassa\*, Amba Jean Chills

Laboratory of Research E3M, Department of Civil Engineering, National Higher Polytechnic School of Douala, University of Douala, Douala, Cameroon

## Email address:

daniel.zoa77@yahoo.fr (Z. Ambassa), jeanchills@yahoo.fr (A. J. Chills)

\*Corresponding author

## To cite this article:

Zoa Ambassa, Amba Jean Chills. Numerical Finite Element Analysis of the Soil Mass Subjected to the Impulsive Load of a Standard Penetration Test (SPT): Assessment of Young's Modulus of Soils. *American Journal of Civil Engineering*. Vol. 10, No. 3, 2022, pp. 88-108. doi: 10.11648/j.ajce.20221003.12

Received: April 1, 2022; Accepted: April 22, 2022; Published: May 26, 2022

---

**Abstract:** In this paper, we propose a method for the direct determination of the Young's modulus of soils from the Standard Penetration Test by performing back-calculations iteratively knowing the reference sinkage which is 30 cm. We modeled the Standard Penetration Test taking into account the experimental protocol in the field and the typical Impulsive load subjected in the soils mass. Numerical simulations have been carried out using the Finite Element calculation code Cast3M in 2-D axisymmetric. For all the calculations, the Poisson's ratio was taken as equal to 0.3 for the soil and a unit weight of all the soils set at 17 kN/m<sup>3</sup>. The influence of the drilling diameter was taken into account, with two modeled pre-drilling diameters, 65 and 200 mm. From these dynamic calculations at small time steps, carried out in a semi-infinite soil mass without natural water content, it appears that the Young's modulus of the soils determined by our method, strongly depends on the number of blows at the SPT of the test depth and the diameter of the borehole. Tables, charts for practical use and a direct relationship for determining the Young's modulus of soils subjected by SPT by this method have been established and proposed in this paper function of the number of blows at the SPT.

**Keywords:** Soil Mass, Standard Penetration Test, Impulsive Load, Numerical Simulation, Young's Modulus

---

## 1. Introduction

In this paper, we propose a method for the direct determination of the Young's modulus of soils from the Standard Penetration Test by performing back-calculations iteratively knowing the reference sinkage which is 30 cm. The study begins with a well-defined methodological basis with analytical equations allowing on the one hand to determine the impact force at the top of the drill string as a function of the experimental signal; then, one presents the dynamic solution starting from an incremental calculation with small steps of time. The modeling of the dry soil mass, pre-drilled, solicited by an impulsive load from the SPT is made from the Finite Element calculation code Cast3M [1]. Series of more than 500 numerical simulations were made, with values of the blows of the SPT ranging from 1 to 100, and a variable test depth from

1 to 20 m. The influence of the drilling diameter was taken into account, with two modeled pre-drilling diameters, 65 and 200 mm. The assumptions made, the main principles of our modeling and the results obtained are presented in this article, of which a basic concepts for the design geotechnical's structures is briefly described.

## 2. Basic Concepts for the Design Geotechnical's Structures

### 2.1. Basis of Design of the Geotechnical's Structures

In the already long history of soil mechanics, heated discussions have pitted the proponents of calculation methods for geotechnical structures derived directly from mechanics (continuous media and solids) against the supporters of

methods derived from the use *in situ* tests (penetration tests, deformation tests and geophysical tests). The traditional methods for calculating foundations (in c: shear strength and  $\phi$ : friction angle) have the advantage of being known in all countries, sometimes with local variations; they have, on the other hand, the advantage of using the same parameters as retained walls calculations or slope stability calculations and of extending naturally into the numerical calculation methods. Calculation methods from in-situ tests have proven themselves for deep and shallow foundations, and in the rules for calculating foundations for civil engineering structures they have received a monopoly position, while they coexist with traditional methods in the rules applicable to the foundations of buildings. In these studies, the calculation methods are only one element: values must be given to the calculation parameters, whether they are Mohr-Coulomb parameters or the results of in situ tests. Unfortunately, experience shows that the properties of soils are poorly known and often underestimated by poorly conducted or too few tests. The basic tests for the description of soil behavior laws are the oedometric test and the triaxial test. The interpretation of the results of the in situ tests in terms of behavior laws is difficult, because these tests are not homogeneous and the state of the stresses is not generally known. Most foundation calculation methods have been established for conventional working loads, i.e. for failure loads, assigned a safety factor of 2 or 3. Case of simple and classic foundations for which empirical methods have been established, numerical methods can be used to study more complicated geometric configurations. At present, these numerical methods are widely used, especially during large, difficult or expensive projects. The application of numerical methods to geotechnics is constantly growing and significant research efforts are devoted to it around the world. For the practical resolution of soil-foundation-structure interaction problems, and in particular the calculation of displacements of shallow foundations [2-8], numerical methods have many advantages. An interesting aspect should be noted, which makes it easier to implement these methods in the case of shallow foundations: these are the initial stresses prevailing in the soil as well as its intact or altered state, once the foundation has been built, but before application of the loading by the structure. We can, at least for loosely embedded foundations, assume that the stresses are equal to those of the ground at rest and that the ground still has its characteristics intact. The most delicate point for the application of numerical methods to the study of soil-structure interactions is obviously the definition of the behavior of the foundation soil. This definition can be done either in the form of simple characteristics (of the Young's modulus and Poisson's ratio type, in the case where isotropic linear elasticity is chosen), or in the form of equations or rheological models more or less sophisticated. In practice, the rules of justification of the foundations lead to limit the loads applied and one is often in the pseudo-linear field of the behavior load-settlement, justifiable of a modeling of the ground by a continuous isotropic linear elastic medium. The ground is modeled as a continuous medium, thus allowing deformations to be taken into account according to the two or

three dimensions of the problem; the modeling of the ground by a continuous medium is to be opposed to the "one-dimensional" modeling by independent springs (Winkler's model), linear or not, which ignores any interaction between the soil columns and only ensures continuity through the supported structure; these interactions mean that it is not possible, in the case of shallow foundations, to define a modulus reaction (the unidimensional stiffness of the springs) having an intrinsic significance to the ground.

More precise methods, such as numerical calculations, must be used when the soil-structure interaction has a dominant influence. Numerical methods have the ability to take into account macroscopic soil heterogeneities (layers with different characteristics or heterogeneity in plan); the same applies to the heterogeneity caused by different loading levels depending on the points of the soil mass, in the case of a soil with non-linear behavior (variable stiffness). The contact surface between the ground and the supported structure can be represented with various physical characteristics (perfect contact, smooth, rubbing, etc.). The geotechnical structure can be taken into account with its real rigidity, rigidity which conditions, at priori, just as much as the rigidity of the ground, the distribution of the loads and displacements; this leads to more realistic calculations of the differential settlements than the classical approximations of an infinitely rigid foundation or of an infinitely flexible foundation which leads to an overestimation of differential settlements. Numerical methods make it possible to take into account any loading geometries, as well as the staged construction or the progressive application of the loading; they are also well suited to situations where it is necessary to study the interaction between neighboring structures, i.e. where one or more structure-soil-structure interaction problems are involved. This study therefore responds to this problem, that of obtaining the elastic parameters of the soil from the in situ tests, making it possible to feed the elastic calculation models implemented in codes or software for the numerical calculation of geotechnical structures. The advantage of such a method comes from the fact that despite the advantage offered by laboratory tests for the description of the behavior of soils, it is sometimes impossible to obtain an intact sample of saturated clays or loose sands to be able to carry out the laboratory tests. In such sites, only in-situ tests are capable of providing the desired size to size the structure that will be built on the site. In this paper, we develop a method for determining the elastic parameters of soils from the inverse dynamic analysis of the SPT whose use is widespread in the world. With the constantly growing emergence of Finite Elements calculation codes, many engineers and researchers make calculations of geotechnical's structures from a profile of modulus of the ground in place based on complex numerical modeling taking into account the geometry, of the soil-structure interface, staged construction and variable or non-variable loading where they deal with the problem of deformation by applying to this model behavior laws based on linear elasticity, using a "correlation" between the parameters of the in situ tests and a Young's modulus.

## 2.2. Field of Use and Experimental Protocol of the Standard Penetration Test

The Standard Penetration Test applies to fine and grainy soils whose average dimension of the elements does not exceed 20 mm [9]. It consists in determining discontinuously the resistance to dynamic penetration of a standardized corer driven at the bottom of a prior drilling. We count the number of blows required to drive the corer to a certain depth. Once full, the corer is raised to the surface, emptied of its core and then lowered to the bottom of the borehole. The operation is repeated over the entire height of the profile to be tested [9]. The test makes it possible, on the one hand, to draw a penetration profile and, on the other hand, to provide reworked soil samples which can be used to recognize the horizons crossed and on which identification tests can be carried out (particle size, Atterberg limits and water content). The core barrel, placed at the bottom of a preliminary borehole, is driven using a drill string (Figure 1). The borehole can have a diameter varying from 65 mm to 200 mm [10, 11].

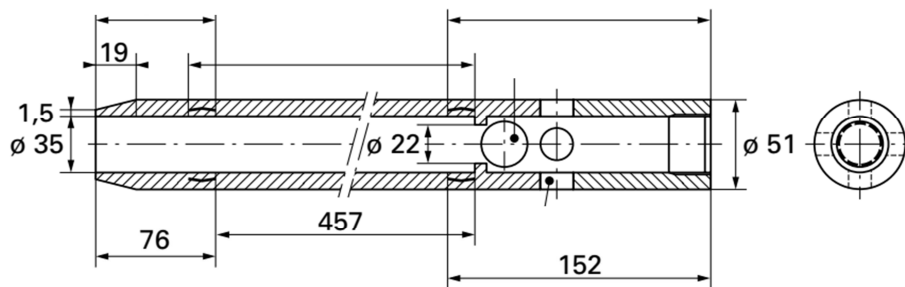
Driving is carried out in successive passes using a hammer of 63.5 kg which falls in free fall from a height of 76 cm on to the head of the drill string. The hammer falls at a beating

rate of 15 to 30 strokes per minute. The depth of each penetration pass is 45 cm. Refusal is considered to have been achieved when one of the following situations is observed during threshing [9]:

- 1) A sinking of the corer of less than 15 cm for 50 blows;
- 2) A sinking of the corer of less than 30 cm for 100 blows;
- 3) A beating of 10 successive blows for zero penetration.

During the beating, three successive depressions are noted:

- 1) The sinking of the installation: it is the sinking of the corer under its own weight and under that of the drill string and the driving device; penetration is continued immediately if this first penetration exceeds 45 cm;
- 2) Initiation sinking: the corer is sunk 15 cm under the effect of  $N_0$  hammer blows;
- 3) Test driving: the corer is driven twice 15 cm under the effect of  $N_1$  then  $N_2$  hammer blows. The number  $N_{SPT} = N_1 + N_2$  is called resistance to penetration (at the standard corer). The results of the sounding are presented in the form of a table and possibly in the form of a curve of variation of  $N_{SPT}$  as a function of depth. The standards specify that the test only applies to soils whose dimension of the largest elements does not exceed 20 mm, whose  $N_{SPT}$  value is between 0 and 100 and for investigation depths not exceeding 50 m.



dimensions in mm

Figure 1. Longitudinal section of the corer.

SPT are carried out quite intensively in several countries around the world and empirically to determine the bearing capacity of shallow and deep foundations as well as for the assessment of the risk of soil liquefaction in seismic zones. They are also used, through correlations, for the determination of the undrained shear strength  $c_u$  of clays, the internal friction angle  $\phi$  [11-15], the soil density index  $I_D$  of pulverulent soils as well as the determination of the propagation velocities of shear seismic waves  $V_s$  [16, 17] and the Young's modulus of soils [18]. To our knowledge, there is no study at present, making it possible to directly obtain the modulus of soil deformation from the SPT.

## 3. Methodology

Although the characteristics of artificial materials such as concrete and steel are well understood, there is no clear method for determining the characteristics of the soil to be introduced into the proposed calculation methods. Indeed, the ground presents a spatial heterogeneity. The variation with

depth of its properties due to anisotropy makes it difficult to model, especially if geotechnical investigations are limited. However, if we consider that the soil has an elastic behavior and that this depends only on its elastic modulus, we are faced with the problem of determining its exact value. Indeed, there is no single Young's modulus for a soil [12, 19, 20]. Moreover, the work of Philipponnat and Hubert [21] demonstrates through its introductory figure, that there are on a single soil sample, an infinity of "modulus of deformations". When the projection of the abscissa of any point coincides with the projection of half the failure stress (stress-strain curve of a soil sample), we have the  $E_{50}$  modulus of the PLAXIS programs [22]. In view of the above, this study is based on the resolution in elasticity of the behavior of slender bodies during their beating in the soil mass by imposing a vertical displacement at the point of contact between the slender rigid body and the soil mass, depending on the number of strokes which will be the design criterion, the Young's modulus of the soil which satisfies this elastic behavior is determined.

### 3.1. Back-calculation Analysis of the SPT

The objective of the back-calculation is to determine the Young's modulus of each slice of soil according to the number of blows to the SPT allowing to obtain a depression of 30 cm. This involves solving a dynamic problem with a vertical impulsive load  $P(t)$ , depending on the time which punches the soil mass characterized by its vertical stiffness. This method is commonly used for the evaluation of the mechanical parameters of civil engineering works during their operation, the primary data of which was collected from non-destructive tests [23-26].

#### 3.1.1. Determination of the Amplitude of the Impulsive Load of the SPT from the Theory of Beating of Slender Bodies

The impact of the hammer on the drill string during driving induces a stress wave at the head of the drill string

propagating with a velocity of  $C_1$ . An assumption is made that the drill string is covered with a helmet so the role is to protect the head from direct successive collisions with the hammer, as well as a distribution of the stresses at the head. The assessment of this axial stress induced by the shock at the head of the drill string, as well as the duration of the shock is carried out according to the test protocol and the experimental signal of the dynamic loading. The helmet is considered as an elastic material having a length  $L_c$ , a Young's modulus  $E_c$  and an area  $A$ , which can be schematized by a spring having a stiffness  $K$  equal to:

$$K = \frac{E_c \cdot A}{L_c} \quad (1)$$

The expression for the vertical velocity at the head of the drill string proposed by Bouafia [27] is defined as follows:

$$\frac{dv_p^0}{dt} = \left[ \frac{2n}{\sqrt{p^2 - n^2}} \left( v_0 - \frac{ng}{p^2} \right) \sin \left( t \sqrt{p^2 - n^2} \right) \right] e^{-nt} - \left[ \frac{2ng}{p^2} \cdot \cos \left( t \sqrt{p^2 - n^2} \right) \right] e^{-nt} + \frac{2ng}{p^2} \quad (2)$$

The compressive stress at the head of the drill string is given by:

$$\sigma_p = \sqrt{E_p \rho_p} \cdot \frac{dv_p^0}{dt} \quad (3)$$

This stress becomes maximum after a time  $t^*$  such as:

$$\left. \frac{\sigma_p}{dt} \right|_{t=t^*} = 0, \text{ which implies } t^* = \frac{1}{\sqrt{p^2 - n^2}} \tan^{-1} \left( \frac{v_0 \sqrt{p^2 - n^2}}{nv_0 - g} \right) \quad (4)$$

In these expressions,  $v_0$  is the initial falling velocity of the striking mass:  $v_0 = \sqrt{2gH}$ ;  $g$ , gravity acceleration;  $H$ , drop height of sheep;  $M$  is the mass of the hammer;  $\rho_p$ , the density of the steel and the coefficients  $n$  and  $p$ , having the dimension of a proper pulsation (rad/s), are defined as follows:

$$n = \frac{K}{2A \cdot \rho_p \cdot C_1} \quad (5)$$

$$p = \sqrt{\frac{K}{M}} \quad (6)$$

The duration of the strock  $t_c$ , corresponds to the first zero of equation (2). Beyond  $t_c$ , equations (2) and (3) lose all physical signification. The analysis carried out here corresponds to a length of the drill string greater than half the distance traveled by the incident wave during the duration of the shock, i.e.  $\frac{t_c C_1}{2}$  [27].

This analysis corresponds to the case where the proper pulsation  $n$  is less than  $p$ . The signal of the stress at the head of the drill string during the impact, manifests a maximum for a time  $t^*$ . Obviously, equation (2) is valid to describe the curve between the first two zero, which corresponds to the duration of the

strock. In the absence of the helmet, and noting by  $A_M$  the cross-sectional area of the hammer, the shock induces at the head of the rod string a velocity such that:

$$dv_p^0 = \frac{v_0}{1 + \frac{A}{A_M}} \quad (7)$$

The compressive stress at the head of the drill string then becomes:

$$\sigma_p = \sqrt{E_p \cdot \rho_p} \cdot \frac{v_0}{1 + \frac{A}{A_M}} \quad (8)$$

Expressions (1) to (8) allow, with practical data, to obtain the loading pressure at the head of the drill string.  $E_p$  is the Young's modulus of the drill string.

#### 3.1.2. Assessment of the Real Amplitude of the Impact Load at the Top of the Drill String

The practical data of the SPT test, that is to say, the falling mass of the sheep (63.5 kg), its height of fall (76 cm) and the resolution of the above equations make it possible to obtain



the values of the parameters entering into the determination of the magnitude of the impact force of the SPT. Table 1 presents the values obtained.

### 3.2. Solving a Problem of the Soil Mass Under Dynamic Loading

The deformation of a soil mass subjected to static loads is calculated by writing the balance between the internal forces and the external forces.

$$Ku = P \quad (9)$$

The field of displacement as well as the calculated forces must check the boundary conditions (embeddings, supports, free edges,...). The equation of motion of a N degrees of freedom soil mass subjected to an impulsive load can be expressed as:

$$M\ddot{u}(t) + C\dot{u}(t) + Ku(t) = P(t) \quad (10)$$

where M, C and K are N x N mass, damping and stiffness matrixes, respectively,  $u(t)$ ,  $\dot{u}(t)$  and  $\ddot{u}(t)$  are respectively, the displacement, the velocity and the acceleration vector, P(t) is the impulsive load from SPT.

Using Taylor's theorem,  $u(t)$  may be represented by a Taylor series:

$$u_{t+\Delta t} = u_t + \Delta t \dot{u}_t + \frac{\Delta t^2}{2} \ddot{u}_t + \frac{\Delta t^3}{6} \dddot{u}_t + \dots \quad (11)$$

$$\dot{u}_{t+\Delta t} = \dot{u}_t + \Delta t \ddot{u}_t + \frac{\Delta t^2}{2} \dddot{u}_{t+\Delta t} \dots \quad (12)$$

Newmark has expressed these functions (11) and (12) as follows:

$$u_{t+\Delta t} = u_t + \Delta t \dot{u}_t + \frac{\Delta t^2}{2} \ddot{u}_t + \beta \Delta t^3 \ddot{u}_t \quad (13)$$

$$\dot{u}_{t+\Delta t} = \dot{u}_t + \Delta t \ddot{u}_t + \gamma \Delta t^2 \ddot{u}_{t+\Delta t} \quad (14)$$

$$\left[ M + \frac{\Delta t}{2} C \right] \ddot{u}_{t+\Delta t} = P_{t+\Delta t} - C \left[ \dot{u}_t + \frac{\Delta t}{2} \ddot{u}_t \right] - K \left[ u_t + \Delta t \dot{u}_t + \frac{\Delta t^2}{2} \ddot{u}_t \right] \quad (20)$$

The resolution of the problem described above will be done by numerical modeling in the follow of this work from the Finite Element calculation code Cast3M [1].

## 4. 2-D Axisymmetric or 3-D Numerical Modeling of the Soil Mass-Corer on Cast3M

### 4.1. Technical Considerations and Presentation of the Numerical Model

In this paper, the modeling of the soil mass, solicited by

The assumption of the linearity of acceleration between two steps of time is written as follows:

$$\ddot{u}_{t+\Delta t} = \left( \frac{\ddot{u}_{t+\Delta t} - \ddot{u}_t}{\Delta t} \right) \quad (15)$$

The substitution of Eq. (15) in (13) and (14) leads to the standard form of Newmark's equations:

$$u_{t+\Delta t} = u_t + \Delta t \dot{u}_t + \left( \left( \frac{1}{2} - \beta \right) \ddot{u}_t + \beta \ddot{u}_{t+\Delta t} \right) \Delta t^2 \quad (16)$$

$$\dot{u}_{t+\Delta t} = \dot{u}_t + \left( (1 - \gamma) \ddot{u}_t + \gamma \ddot{u}_{t+\Delta t} \right) \Delta t \quad (17)$$

$\Delta t$  is the incremental time,  $\beta$  and  $\gamma$  are the Newmark's parameters. Depending on the values that affect, they will play important role in the nature of temporal integration scheme. In fact to ensure the explicit character of the

Newmark's scheme, we must have  $\beta = \frac{1}{4}$  and  $\gamma = \frac{1}{2}$  in Eq.

(16 and 17). To ensure the stability of the scheme with  $\beta = \frac{1}{4}$ , we must have  $\gamma > 0.5$ . However, the scheme becomes dissipative for  $\gamma > 0.5$  [1].

So the resolution of the dynamic problem is done with the help of a 2-D axysymmetric or 3-D model and explicit algorithm of Newmark (average acceleration). The average acceleration algorithm is particular case where  $\beta = \frac{1}{4}$  and  $\gamma = \frac{1}{2}$ . The name of the average acceleration becomes from the equality:

$$u_{t+\Delta t} = u_t + \Delta t \dot{u}_t + \frac{\Delta t^2}{2} \ddot{u}_t \quad (18)$$

$$\dot{u}_{t+\Delta t} = \dot{u}_t + \frac{\Delta t}{2} \ddot{u}_t + \frac{\Delta t}{2} \ddot{u}_{t+\Delta t} \quad (19)$$

Which leads to:

the sinking of the core barrel (Figure 2) at the bottom of the borehole, was carried out by considering two diameters of the borehole: 65 and 200 mm [10, 11]. The choice of an axisymmetric two-dimensional modeling for the behavior of the soil-corer body is justified by the symmetry of the problem and the fact that the three-dimensional modeling involves a substantial computation time. In order to best respect the conditions due to a semi-infinite Boussinesq soil mass [28], a very extensive mesh was adopted while trying to remain within a reasonable number of degrees of freedom. During a Finite Element calculation, in addition to the type of elements used and the boundary conditions, the level of precision of the results depends mainly on the fineness of the

mesh and the cut-off frequency for a dynamic calculation. Thus, a finer mesh was chosen in the vicinity of the core barrel loading zone and in the surface layer; places where large stress and strain gradients are expected. The mesh

becomes coarser with the distance from these zones. Table 1 presents the parameters used to obtain the maximum pressure to be applied at the top of the corer to resolution and application of equations (1) to (8) above.

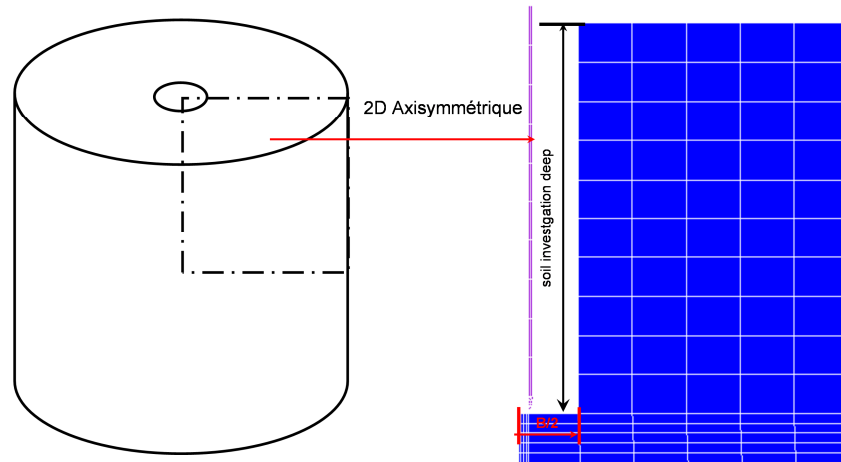


Figure 2. Pre-drilling of the soil mass for the insertion of the corer and 2-D axisymmetric consideration.

Table 1. Calculated pressure to apply the corer head.

Hammer Mass (kg)	Corer exterior diameter (cm)	Corer interior diameter (cm)	H: Length of falling of hammer (m)	$g$ (m/s <sup>2</sup> )	$q$ (MPa)
63.5	5.1	3.5	0.76	10	139.15

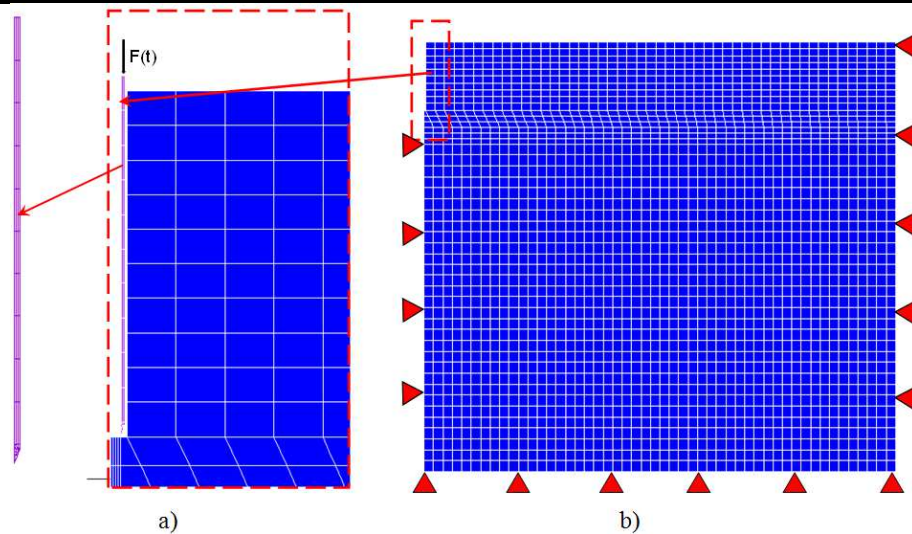


Figure 3. a) details of the position of the corer downhole and view of the corer; b) 2-D view of the mesh of the axisymmetric model of the soil mass with corer positioned at the bottom of the hole and standard fixities.

#### 4.2. Solving the Problem in 2-D Axisymmetric and 3-D

Being able to model a soil mass of infinite extent only in a finite way in a Finite Element approach, the phenomenon of reflection of the waves on the boundaries for the dynamic calculation is then an important problem. To deal with this problem, artificial boundaries (called absorber bands) are used on the edges (vertical and lower) of the model to describe the influence of the external environment and limit the influence of the boundaries and avoid parasitic reflected waves [23-26]. The taking into account of the boundary conditions of the modeling in 2-D axisymmetric mode implies a fixation of displacements according to the radial

direction of the border located on the vertical axis of symmetry. Figure 3 shows the views of the 2-D mesh (5 meters on each side) of the soil mass solicited by the corer at the bottom of a hole previously made from the Finite Element calculation code comprising 3239 elements QUA8 quadrangles and 9976 knots. For this dynamic calculation under Cast3M [1], cut-off frequency of 750 was chosen.

Figure 4 presents the 3-D view of the mesh of the solid-core half-model, made up of cubic elements with 8 nodes (CUB8), with 132549 nodes and 124150 elements. The modeling is done incrementally at small time steps corresponding to the total loading signal which is a function of the number of hammer strokes which fall on the drill string of the corer. The

incremental numerical modeling at small time steps is carried out by respecting the principles of equations (9) to (20). The impulse pressure at the top of the corer is 139.15 MPa (Table 1). The mechanical and geometric characteristics of the soil-corer mass assembly analyzed are summarized in Table 2. The soil-corer mass assembly has a linear, homogeneous and

isotropic elastic behavior. This numerical modeling obeys the SPT protocol. The simulation is carried out iteratively by assigning to the slice of the ground a Young's modulus which allows, depending on the number of blows programmed from the loading signal of a blow, to obtain a displacement of 30 cm at the point application of the corer.

**Table 2.** Mechanical and geometric characteristics of the soil-corer assembly.

Material	Thickness (cm)	Young's (MPa)	Poisson ratio	$\rho$ (kg/m <sup>3</sup> )	Vertical displacement function of a number of blows at the SPT (cm)
Soil mass	Semi-infinite	?	0.3	1700	
Corer	0.775	210000	0.1	8750	30

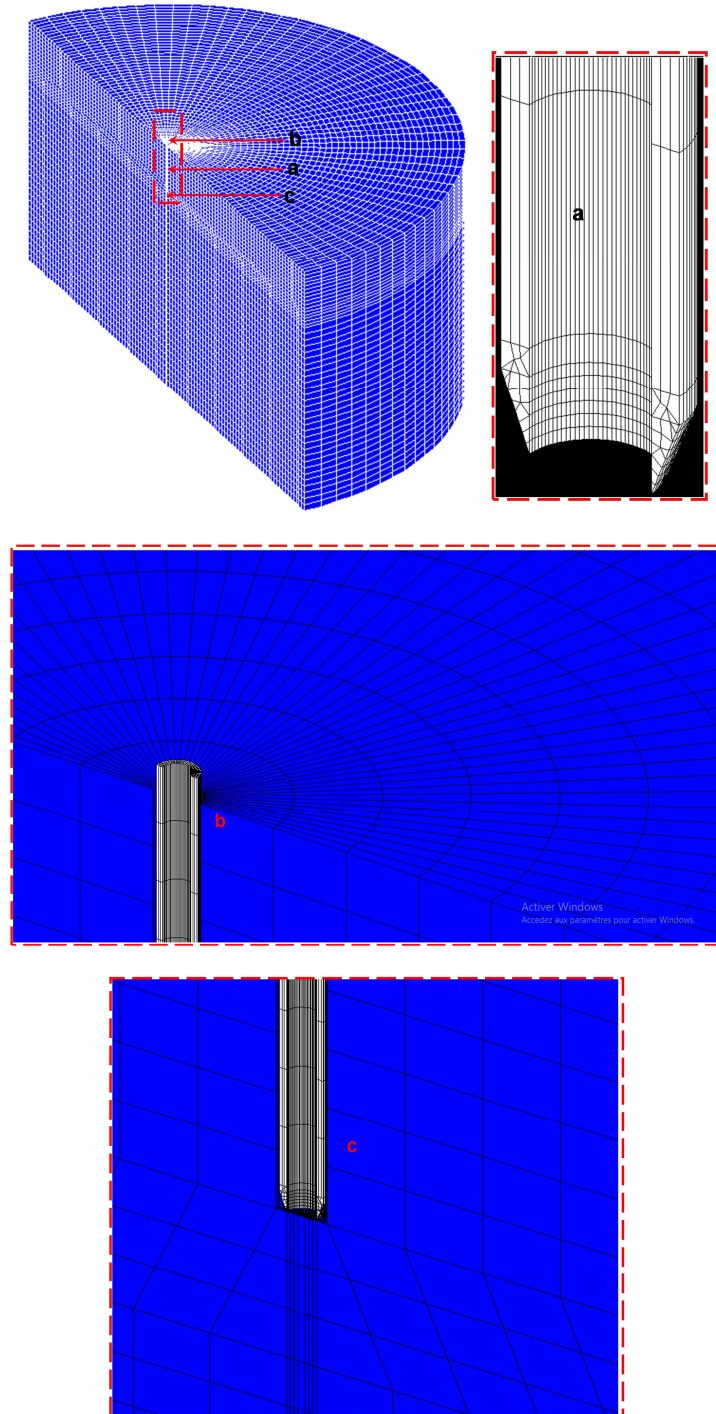


**Figure 4.** 3-D view of the mesh of the  $\frac{1}{2}$  model of the soil mass with corer positioned at the bottom of the hole with all the details of the mesh zones.

## 5. Numerical Calculation Results

The loading signal under a ramming stroke in soil mass as a function of time ( $10^{-2}$  s) at the head of the corer was reconstructed and used for the calculation, the typical shape of this drill string loading signal above the corer is shown in Figure 5 [27], below and programmed in the Finite Element

calculation code Cast3M [1] for our dynamic calculations. Having noted that the duration of a calculation was enormous to be able to obtain results and given the number of numerical simulations necessary for this study, we gave up the use of our 3-D model in favor of the 2-D axisymmetric model which we presented in the previous part.

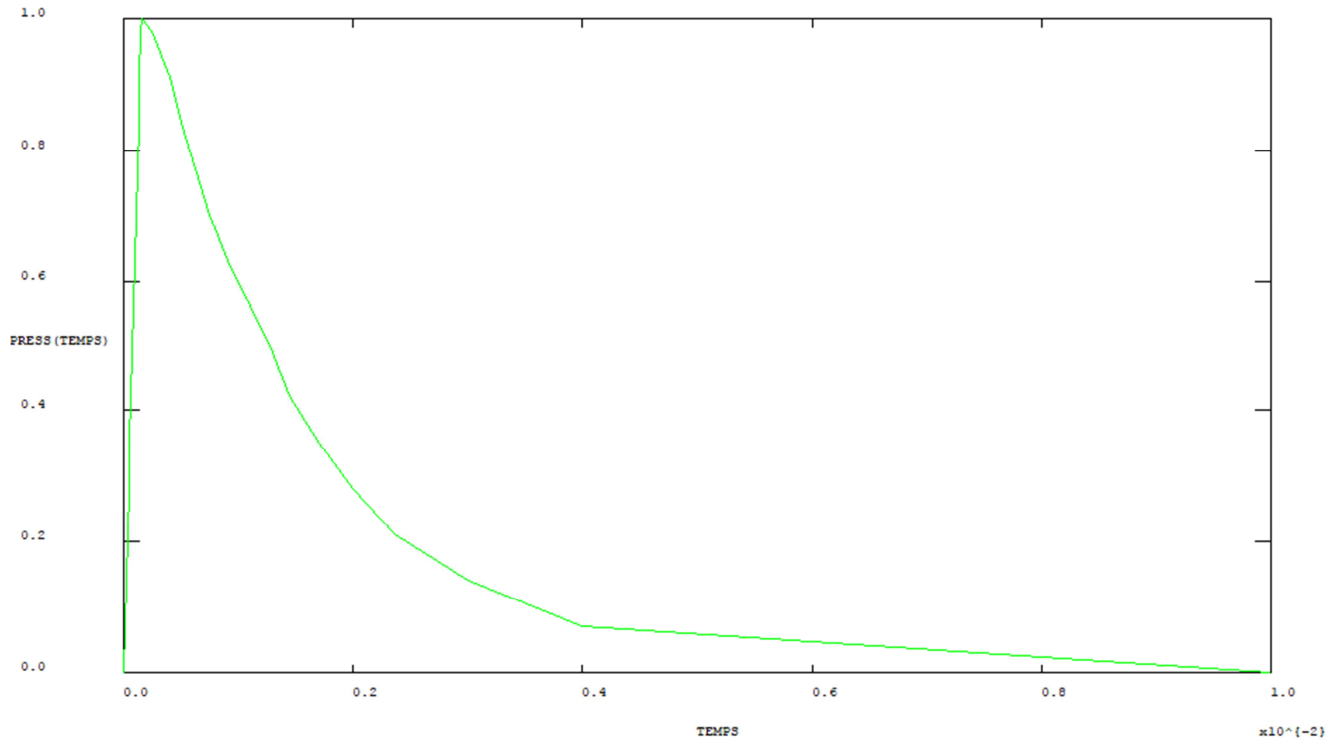


**Figure 5.** Typical pattern of the loading signal at the head of the corer under a driving blow during the SPT in soil mass.

Figure 6, represents the deformed of the axisymmetric 2D mesh which highlights the punching of the soil by the corer, after a dynamic calculation. It is clearly shown through figure 7 that the walls of the split corer penetrate the ground (30 cm) while the displacement in the center is 15.2 cm.

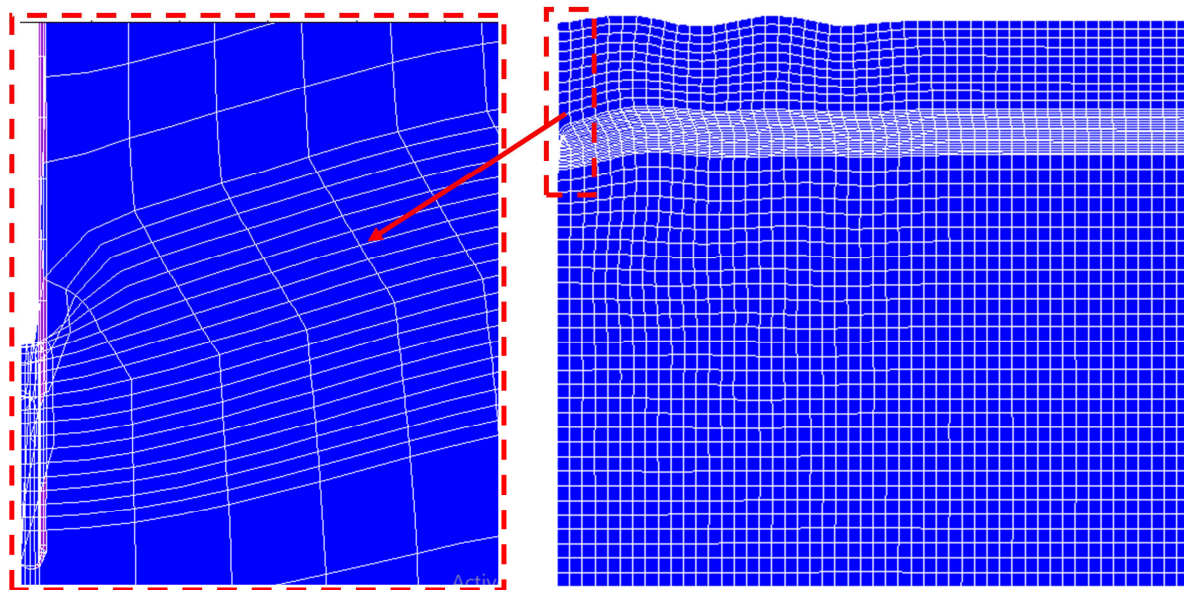


**Figure 6.** 2-D Deformed mesh after incremental calculation at small time steps (1<sup>st</sup> stroke of the SPT test over a series of 30 strokes at time: 0.01s).

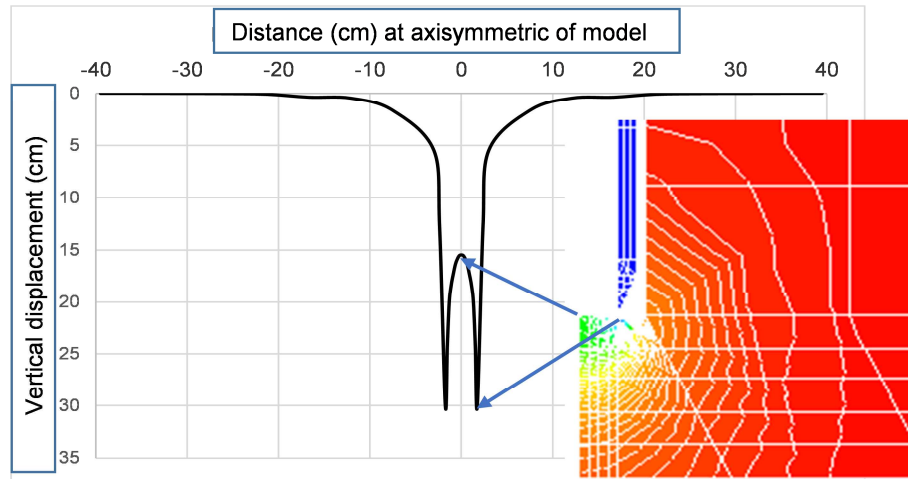


**Figure 7.** Pattern of the vertical displacement of the soil mass at the points of contact with the corer and at the vertical axis of the axisymmetric 2D model (one stroke of the SPT test at time: 0.01s).

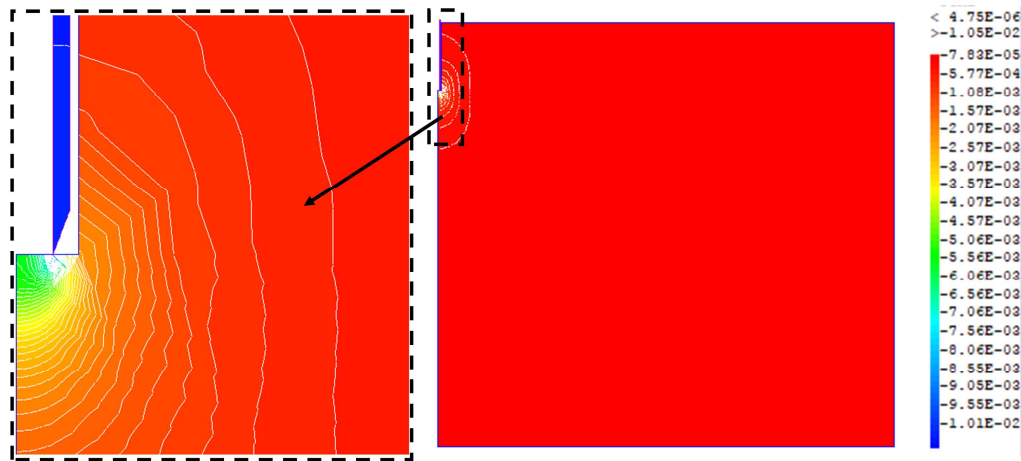


**Figure 8.** Mapping of vertical displacements (m) in the model after incremental calculation at small time steps (1<sup>st</sup> stroke of hammer of the SPT over a series of 30 strokes at time: 0.002s).

The displacement curves and the cartography of the strains, stresses and vertical displacements resulting from the various modelings are presented through figures 7 to 18. These figures shows that the fields of displacement, strains

and stresses are maximum at the point of contact of the corer with the soil mass. This punches the ground (figure 7). In all the numerical simulations carried out, the water table was absent in the soil mass.

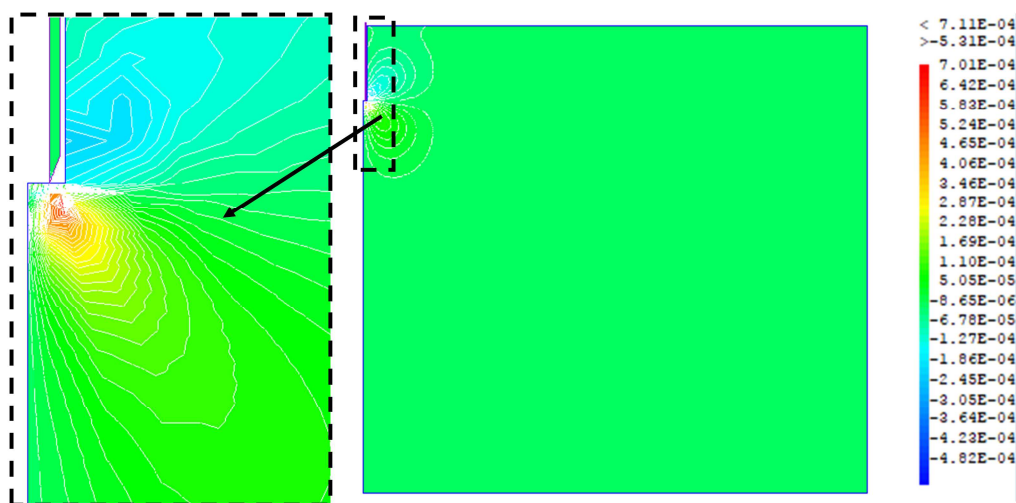


**Figure 9.** Mapping of the radial displacement (in meters) in the model after incremental calculation at small time steps (1<sup>st</sup> stroke of the hammer of the SPT over a series of 30 strokes at time: 0.002s).



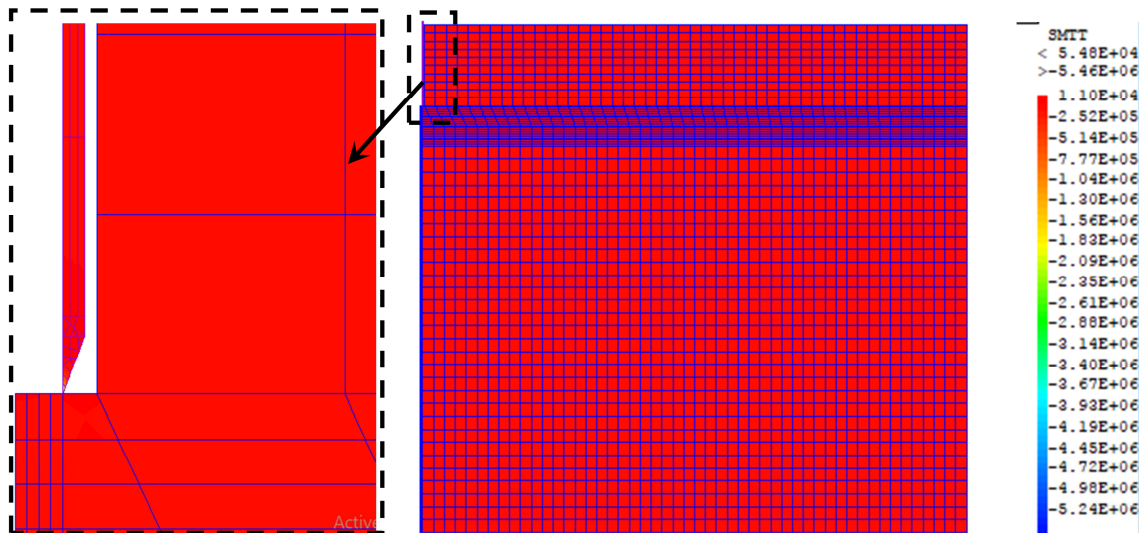


**Figure 10.** Map of ortho-radial stresses (in kPa) in the model after incremental calculation at small time steps (1<sup>st</sup> stroke of the hammer of the SPT over a series of 30 strokes at time: 0.002s).

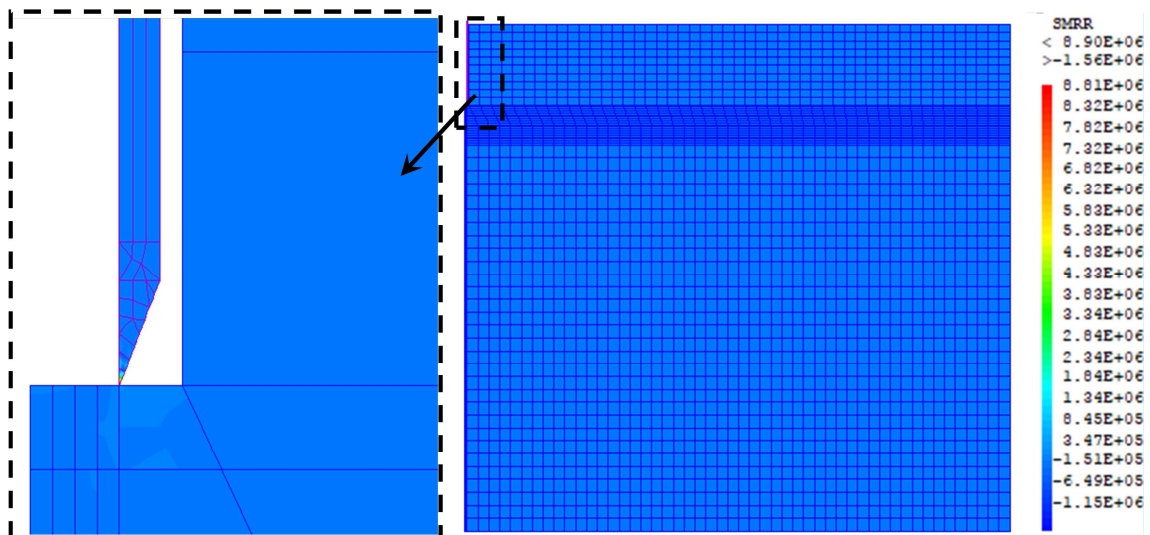


**Figure 11.** Map of radial stresses (in kPa) in the model after incremental calculation at small time steps (1<sup>st</sup> stroke of the hammer of the SPT over a series of 30 strokes at time: 0.002s).

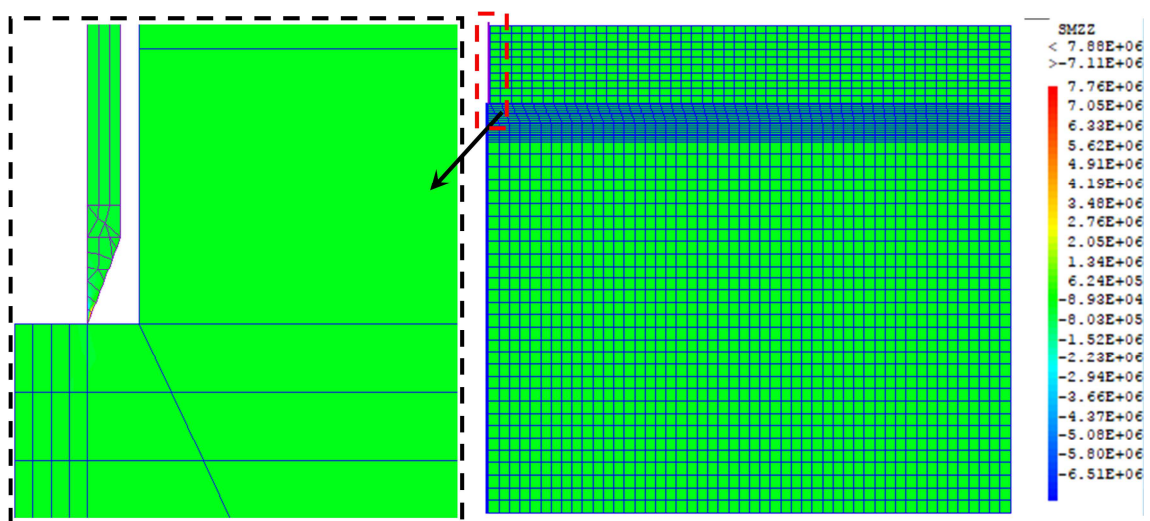


**Figure 12.** Map of vertical stresses (in kPa) in the model after incremental calculation at small time steps (1<sup>st</sup> stroke of the hammer of the SPT over a series of 30 strokes at time: 0.002s).

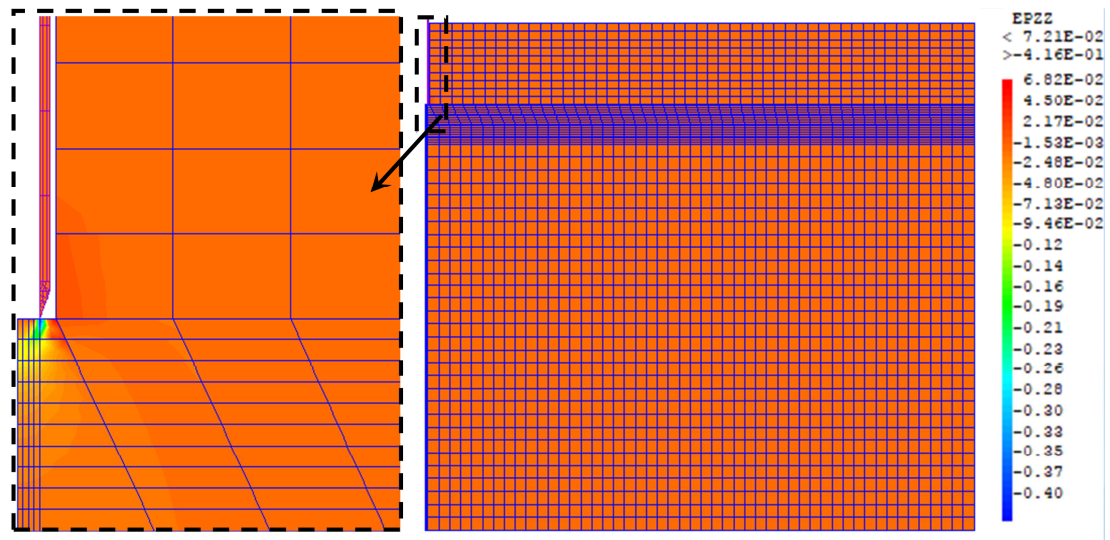


**Figure 13.** Map of vertical strains in the model after incremental calculation at small time steps (1<sup>st</sup> stroke of the hammer of the SPT over a series of 30 strokes at time: 0.002s).

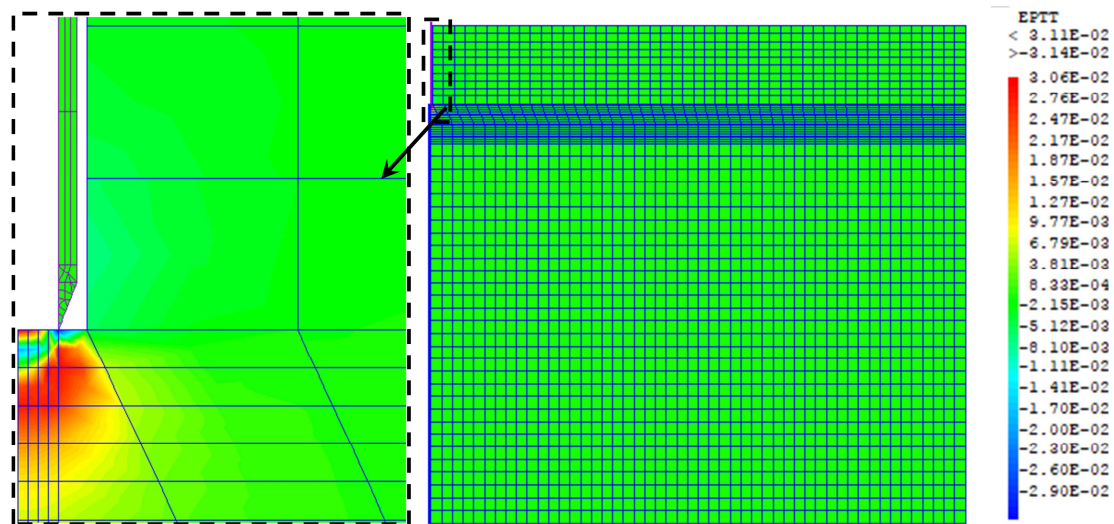


**Figure 14.** Mapping of ortho-radial strains in the model after incremental calculation at small time steps (1<sup>st</sup> stroke of the hammer of the SPT over a series of 30 strokes at time: 0.002s).

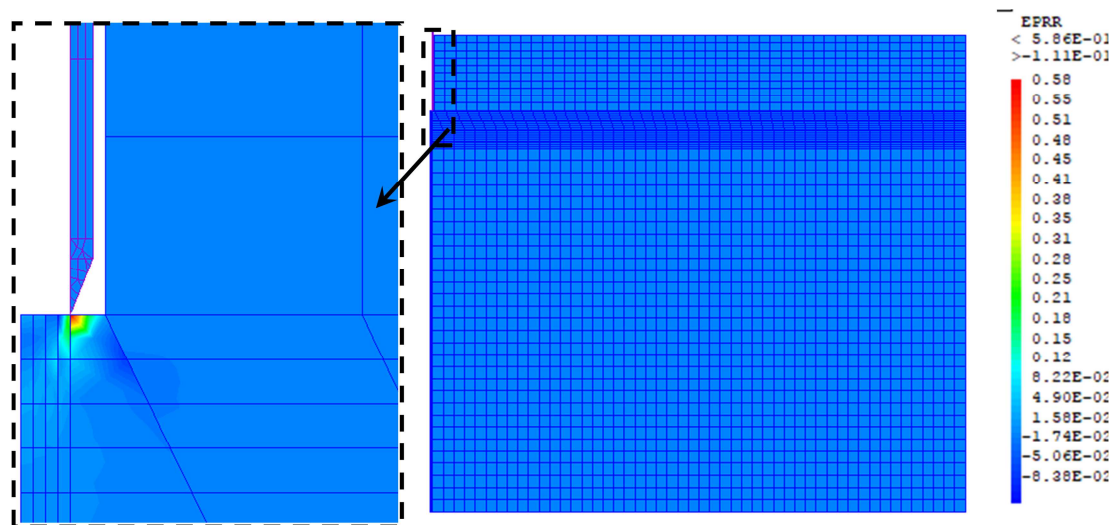


**Figure 15.** Mapping of radial strains in the model after incremental calculation at small time steps (1<sup>st</sup> stroke of the hammer of the SPT over a series of 30 strokes at time: 0.002s).

Figures 13 to 15 show that the strain levels obtained in the model after the incremental dynamic calculation at small time steps are consistent with those of the in situ tests. Figure 16 below shows the allowable deformation

levels in the soil mass for each geotechnical structure [4, 8]. For the in situ tests, the subject of this work, the levels of deformation in the soil mass vary from a little less than  $10^{-3}$  to 0.1.

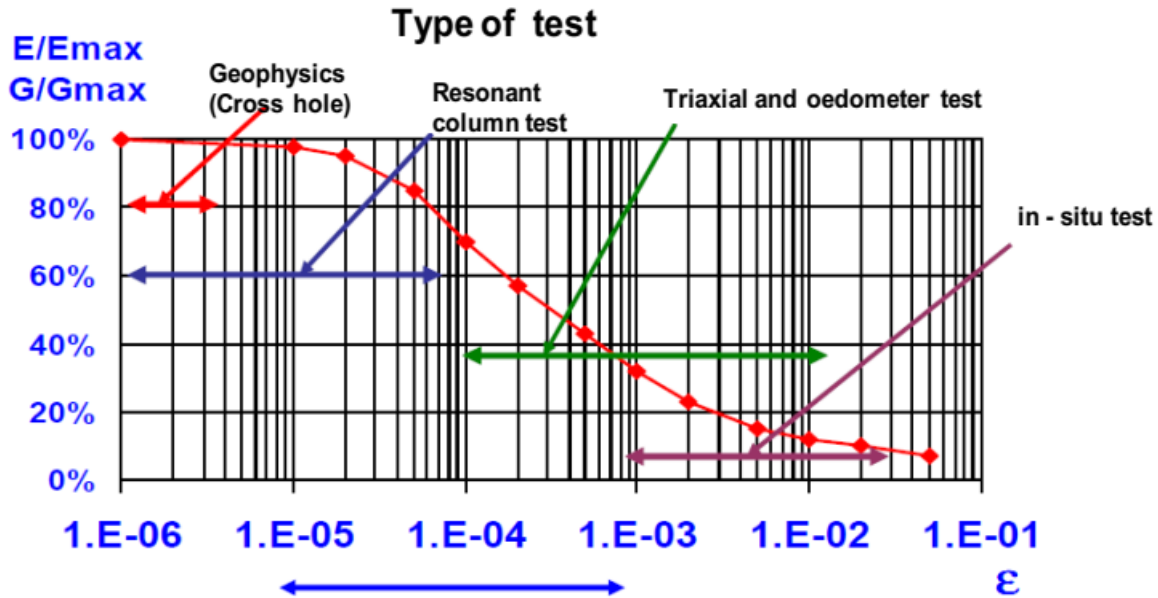


Figure 16. Shear modulus ratio vs strain level of the soils [4, 8].

In this paper, more than 500 numerical simulations were carried out to obtain the results which are presented both in figures 3 to 15 and 17 to 19 and in summary Tables 3 to 5. In this work, hypotheses have been clearly stated followed by a scientific approach respecting the conditions imposed by equations (1) to (20) with the aim of directly obtaining the Young's modulus of the soil mass from a penetration test with a corer. In current practice, several in situ test methods make it possible to directly obtain geotechnical parameters of soils used mainly for the designing geotechnical's structures and the calculation of soil liquefaction. With regard to foundations and embankments, their design requires joint determination of bearing capacity and settlement. Among the in situ tests, apart from the pressuremeter test which directly provides the soil failure parameter (the standard net limit pressure corrected from the total horizontal stress acting in the soil at test elevation  $p_l^*$ ) and the Normalized Menard pressuremeter modulus  $E_M$  [29-31], useful for the direct calculation of settlement, the other in situ tests commonly implemented, only provide the soil resistance parameter (cone resistance  $q_c$ , for the Cone Penetration Test [14, 32-34]; dynamic cone resistance ( $q_d$ ): DHT [35] and the number of blows  $N_{SPT}$  for the SPT [36, 37].

The calculation of the settlement of the geotechnical

structures from the methods derived from these last three tests is carried out using soil deformation moduli obtained by correlation with the resistance parameter provided by each of these tests. In the case of studies of soil-structure interaction or structure-soil-structure interaction, and with the intensive development of computer codes in geotechnical engineering, and the use of high-performance computers; Today, engineers and researchers are increasingly making stress-strain calculations which make it possible to assess the overall behavior of the structure or part of the structure, making it easy to directly control the load corresponding to the allowable settlement [12, 14, 35-39] of said work in the elastic domain. These stress-strain calculation methods do not replace the empirical methods which, moreover, have proved their worth for the calculation of structures, but are used to facilitate the task of engineers and researchers in this field for the validation of their designing and rapid decision-making. These calculation methods are only one element, regardless of the type of in situ tests carried out, the values of the soil deformation parameters must be given. Numerical methods are essential, when we have more complex geometric configurations or when the calculation in staged construction is essential.



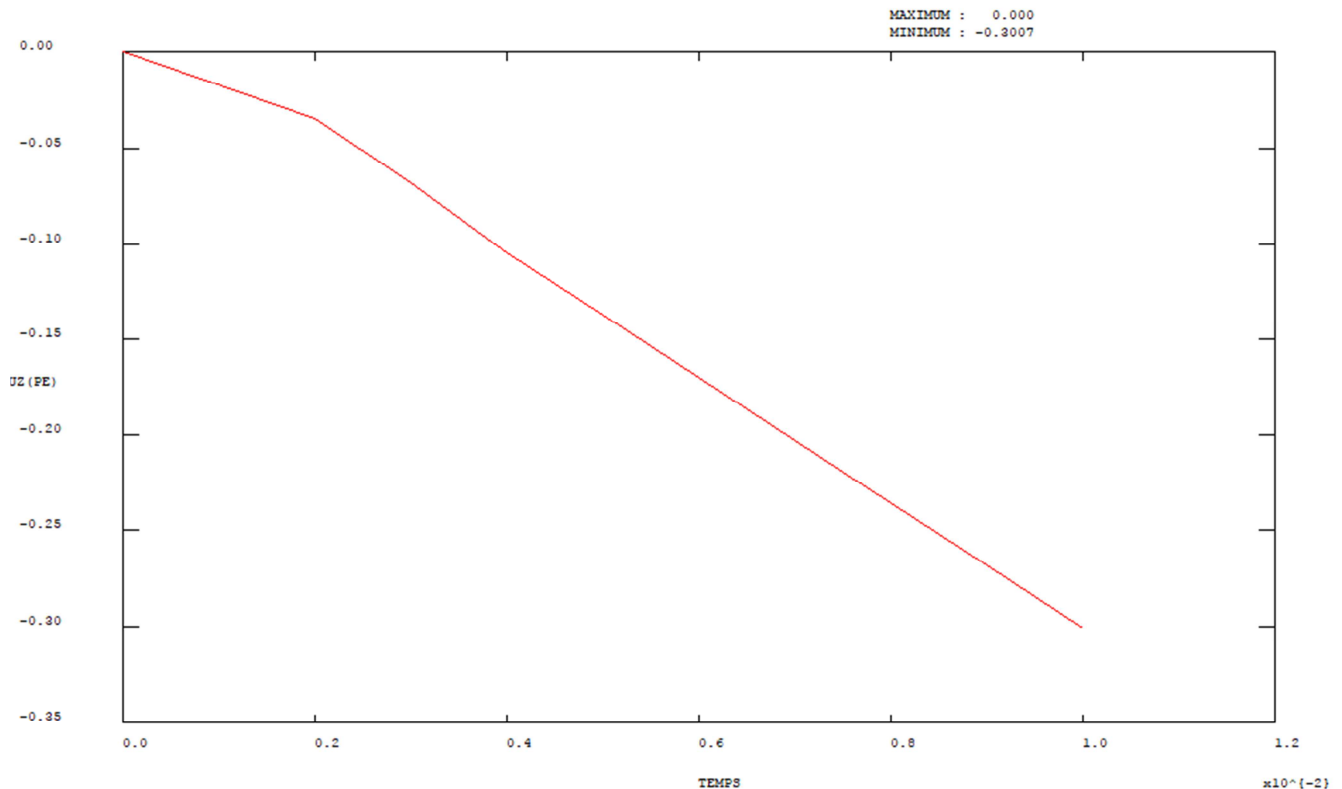


**Figure 17.** Vertical displacement (m) vs time of the soil mass at the point of application of the SPT at the first stroke.

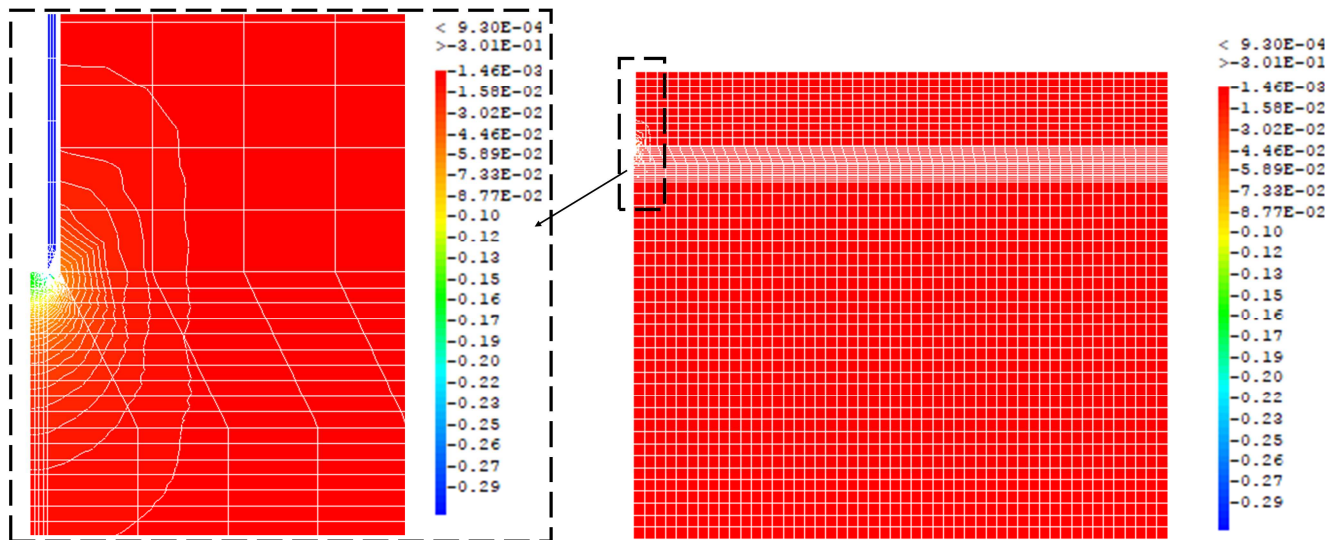


**Figure 18.** Mapping of vertical displacement (m) of soils mass of application of the SPT at the first stroke.

From a complex numerical modeling in backcalculation, the moduli of soil deformation (similar to the Young's modulus) were obtained in this study, according to the number of blows of sheep of the test of penetration test to the corer. Several backcalculations with the number of stroke varying from 0 to 100 were carried out and the values of the moduli corresponding to the number of blows were determined according to the vertical displacement of the corer. From this study, just after an investigation in the field giving the number of  $N_{SPT}$  hits per slice of soil, it suffices to choose the Young's modulus of the soil in tables 3 and 4,

allowing to feed the elastic models implemented in software and professional or research calculation codes.

### 5.1. Influence of the Number of SPT Blows in the Determination of the Young's Modulus of the Soil

The Young's modulus of the soil increases with the increase in the number of strokes giving a displacement of 30 cm. The chart in Figure 19 and Tables 3 and 4 highlight this finding. The modeling was carried out taking into account the number of strokes generally highlighted in this type of test, i.e. from 1 to 100 strokes. It is useful to specify that the

increase in the Young's modulus according to the number of blows, does not necessarily obey a linear law, because it is a dynamic calculation, in which time plays an important role.

### 5.2. Influence of the Loading Time in the Determination of the Young's Modulus of the Soil

The loading time plays an important role in determining the Young's modulus of the soil. Figure 17, Table 3 and 4 highlights this observation, because the displacements verifying the behavior of the soil under the impetus of a load at the head of the drill string are not obtained at the same time increments.

### 5.3. Influence of the Depth of Test in the Determination of the Young's Modulus of the Soil

The Young's modulus of the soil decreases gradually with increasing test depth. Figure 19 and tables 3 and 4 highlight this finding. In this regard, a disturbance on the displacement signal was observed at 5 m depth for the number of strokes ranging from 88 to 100, presenting rather an increase in the Young's modulus of the soil (between 1 and 5 m of depth). For the same borehole diameter (65 mm), at a depth of 1 m, the average  $E/N_{SPT}$  ratio = 10.23; this average ratio is 7.44 at 5 m depth and 1.61 at 20 m depth.

### 5.4. Influence of the Diameter of the Pre-drilling in the Determination of the Young's Modulus of the Soil

It was mentioned in this work that the corer penetration test protocol requires that the test be carried out at the bottom of a borehole with a diameter ranging from 65 to 200 mm. Considering the cost of each calculation, an influence of the borehole diameter on the Young's modulus values was studied by taking into account only the two extreme values, i.e. 65 and 200 mm. The results summarized in Figure 20 and Tables 3, 4 and 5 show that the Young's modulus of the soil decreases with increasing borehole diameter. At 1 m depth and for a borehole diameter of 65 mm, the average  $E/N_{SPT}$  ratio = 10.23; while this average ratio is equivalent to 7.66 for a borehole diameter of 200 mm.

### 5.5. Direct Determination of the Young's Modulus of the Soil from $N_{SPT}$

The simultaneous influence of the number of blows at SPT, the loading time, the test depth and the diameter of the borehole in the determination of the values of the Young's modulus of soils above the water content have been analyzed in detail. In view of the above, in addition to the number of  $N_{SPT}$  hits, two additional parameters strongly influence the determination of the Young's modulus of the soil. This Young's modulus increases with the increase in the number of blows, gradually decreasing as the test depth (D) increases. It also decreases when the borehole diameter (B) increases. A direct relationship linking the Young's modulus  $E(N_{SPT}, D, B)$  of the soils to the influential parameters above is defined as follows:

$$E \text{ (MPa)} = k_N \cdot N_{SPT} \cdot k_D \cdot k_B \quad (21)$$

with,  $N_{SPT}$ : number of blows obtained in the core drill penetration test for a penetration of 30 cm, at each test depth;

$k_N$ : correction factor depending on the number of blows obtained in the core drill penetration test (Table 4). A linear interpolation between two  $N_{SPT}$  values can be performed to obtain intermediate values;

$k_D$ : correction factor depending simultaneously on the depth (soils investigation depth) of measurement and the number of counts. It is equal to 1 for a measurement depth between 0 and 1 m and for any value of  $N_{SPT}$ ; beyond this depth, the corresponding value must be chosen from table 4. A double linear interpolation can be carried out to obtain the values corresponding to the intermediate depths;

$k_B$ : correction factor depending simultaneously on the diameter of the borehole and the number of blows. The diameter of the borehole can vary from 65 to 200 mm depending on the case.  $k_B = 1$  for any value of  $N_{SPT}$  and for a borehole with a diameter of 65 mm, beyond this diameter, the value must be chosen from table 4. A double linear interpolation can be carried out to obtain the intermediate values corresponding to the diameters drilling between 65 and 200 mm.

The formula for determining the Young's modulus above has been translated into charts for practical use (Figures 19 to 20).

Outside the Young's modulus of soils  $E(N_{SPT}, D, B)$ , other additional parameters were obtained such as the dynamic shear modulus (G) of the soils necessary for the calculation of structures in seismic zones or structures exposed to vibrations; the vertical modulus reaction ( $k_v$ ) of soils, the mode of determination of which is derived from the classic formulas for the settlement of surface foundations in elasticity [2, 28, 40-47], (this parameter is necessary for the analytical solution of the behavior of raft foundations, industrial platforms, railway platforms, concrete pavements, etc.); the horizontal modulus reaction of the soils: ( $k_h$ ) calculated according to the recommendations [48, 49], necessary for the calculation of the retaining structures as well as the vertical stiffness  $K_{zz}$  of the layer of soil according to the number of blows at SPT:

$$G = \frac{E_s}{2.6} \text{ in this paper poisson's ratio} = 0.3 \quad (22)$$

$$k_v = \frac{0.65 E_s}{B_1 (1 - \nu_s^2)} \sqrt[12]{\frac{E_s B_i^4}{E_b I_b}} \text{ from [2]} \quad (23)$$

$$k_h = (E_b I_b)^{\frac{1}{3}} \text{ from [49]} \quad (24)$$

For Japanese reglementation, PHRI-TSPHF [44]:

$$k_h = \frac{P}{B_1 Z \sqrt{y}}$$

$$K_{zz} = N_{SPT} \frac{P(t)}{0.3} \quad (25)$$

with,  $B_1$ : width of the footing,  $E_b$ : Young's modulus of the structural element to be designed,  $I_b$ : moment of inertia of the structural element to be designed,  $P(t)$ : impulsive load at the top of the drill string depending on the loading time.

It is important to mention here that the parameters  $X_i$

obtained correspond to the slice of soil of thickness  $H_i$  for which the value of  $N_{SPT}$  was obtained. The average value of each parameter ( $X_m$ ) corresponding to the complete profile of the desired soil can be obtained by the formula below:

$$X_m = \frac{\sum_i^n X_i H_i}{\sum_i H_i} \quad (26)$$

**Table 3.** Values of Young's modulus of soils according to the number of blows at SPT in the borehole diameter = 65 mm and test depth = 1 m.

$N_{SPT}$	$E_s$ (MPa)	$E_s/N_{SPT}$	$G$ (MPa)	$E_{oed}$ (MPa)	Uz max obtained at time (s) (Figure 17)
1	1.78	1.78	0.68	2.40	0.010
2	6.90	3.45	2.65	9.29	0.020
4	23.00	5.75	8.85	30.96	0.034
6	47.00	7.83	18.08	63.27	0.054
8	74.00	9.25	28.46	99.62	0.073
10	100.00	10.00	38.46	134.62	0.093
12	120.00	10.00	46.15	161.54	0.113
14	141.30	10.09	54.35	190.21	0.132
16	187.00	11.69	71.92	251.73	0.152
18	225.00	12.50	86.54	302.88	0.172
20	255.00	12.75	98.08	343.27	0.192
22	285.00	12.95	109.62	383.65	0.212
24	310.00	12.92	119.23	417.31	0.232
26	336.00	12.92	129.23	452.31	0.252
28	359.00	12.82	138.08	483.27	0.272
30	378.00	12.60	145.38	508.85	0.292
32	396.00	12.38	152.31	533.08	0.312
34	413.00	12.15	158.85	555.96	0.332
36	431.00	11.97	165.77	580.19	0.352
38	448.00	11.79	172.31	603.08	0.372
40	459.50	11.49	176.73	618.56	0.392
42	473.00	11.26	181.92	636.73	0.412
44	486.00	11.05	186.92	654.23	0.432
46	498.00	10.83	191.54	670.38	0.452
48	510.00	10.63	196.15	686.54	0.472
50	520.50	10.41	200.19	700.67	0.492
52	530.50	10.20	204.04	714.13	0.512
54	539.50	9.99	207.50	726.25	0.532
56	550.00	9.82	211.54	740.38	0.552
58	559.00	9.64	215.00	752.50	0.572
60	568.00	9.47	218.46	764.62	0.592
62	575.20	9.28	221.23	774.31	0.612
64	582.00	9.09	223.85	783.46	0.632
66	605.00	9.17	232.69	814.42	0.652
68	621.00	9.13	238.85	835.96	0.672
70	650.00	9.29	250.00	875.00	0.692
72	750.00	10.42	288.46	1009.62	0.712
74	794.00	10.73	305.38	1068.85	0.734
76	816.00	10.74	313.85	1098.46	0.754
78	837.00	10.73	321.92	1126.73	0.774
80	853.00	10.66	328.08	1148.27	0.794
82	866.00	10.56	333.08	1165.77	0.814
84	878.00	10.45	337.69	1181.92	0.834
86	888.00	10.33	341.54	1195.38	0.854
88	897.50	10.20	345.19	1208.17	0.874
90	909.00	10.10	349.62	1223.65	0.894
92	915.60	9.95	352.15	1232.54	0.914
94	922.00	9.81	354.62	1241.15	0.934
96	928.50	9.67	357.12	1249.90	0.954
98	936.30	9.55	360.12	1260.40	0.974
100	942.80	9.43	362.62	1269.15	0.994

**Table 4.** Values of Young's modulus of soils and corrective factors according to the number of blows at SPT, borehole diameter and test depth.

N <sub>SPT</sub>	Borehole diameter: 65 mm						Borehole diameter: 200 mm					
	Depth of test: 0.6 m			Depth of test: 5 m			Depth of test: 20 m			Depth of test: 0.6 m		
	E <sub>s</sub> (MPa)	k <sub>N</sub>	Uz max at time (s) (Figure 17)	E <sub>s</sub> (MPa)	k <sub>D1</sub>	Uz max at time (s) (Figure 17)	E <sub>s</sub> (MPa)	K <sub>D2</sub>	Uz max at time (s) (Figure 17)	E <sub>s</sub> (MPa)	k <sub>B</sub>	Uz max at time (s) (Figure 17)
1	1.78	1.78	0.010	0.01	0.006	0.01	0.001	0.0006	0.01	1.1	0.62	0.01
2	6.90	3.45	0.020	0.35	0.005	0.02	0.005	0.0007	0.02	5.3	0.77	0.02
4	23.00	5.75	0.034	0.5	0.022	0.04	0.01	0.0004	0.04	17	0.74	0.034
6	47.00	7.83	0.054	2	0.043	0.06	0.01	0.0002	0.06	35	0.74	0.054
8	74.00	9.25	0.073	20	0.270	0.074	0.01	0.0001	0.08	54.5	0.74	0.073
10	100.0	10.00	0.093	32	0.320	0.094	0.1	0.0010	0.1	74.5	0.75	0.093
12	120.0	10.00	0.113	40	0.333	0.114	0.1	0.0008	0.12	90	0.75	0.113
14	141.3	10.09	0.132	50	0.354	0.134	0.2	0.0014	0.14	105	0.74	0.132
16	187.0	11.69	0.152	58	0.310	0.154	0.2	0.0011	0.16	135.5	0.72	0.152
18	225.0	12.50	0.172	61	0.271	0.174	0.2	0.0009	0.18	165	0.73	0.172
20	255.0	12.75	0.192	65	0.255	0.194	0.2	0.0008	0.2	189	0.74	0.192
22	285.0	12.95	0.212	68	0.239	0.214	0.2	0.0007	0.22	212	0.74	0.212
24	310.0	12.92	0.232	83	0.268	0.234	0.2	0.0006	0.24	232.2	0.75	0.232
26	336.0	12.92	0.252	92	0.274	0.254	0.5	0.0015	0.26	250.5	0.75	0.252
28	359.0	12.82	0.272	155	0.432	0.274	1.5	0.004	0.28	267.5	0.75	0.272
30	378.0	12.60	0.292	192	0.508	0.294	5	0.013	0.3	287	0.76	0.292
32	396.0	12.38	0.312	242	0.611	0.314	20	0.051	0.32	297	0.75	0.312
34	413.0	12.15	0.332	270	0.654	0.334	33	0.080	0.34	312	0.76	0.332
36	431.0	11.97	0.352	295	0.684	0.354	44	0.102	0.36	328	0.76	0.352
38	448.0	11.79	0.372	322	0.719	0.374	55.5	0.12	0.38	342	0.76	0.372
40	459.5	11.49	0.392	347	0.755	0.394	67	0.15	0.4	351	0.76	0.392
42	473.0	11.26	0.412	371	0.784	0.414	75	0.16	0.42	365	0.77	0.412
44	486.0	11.05	0.432	392	0.807	0.434	85	0.17	0.44	375	0.77	0.432
46	498.0	10.83	0.452	415	0.833	0.454	94	0.19	0.46	385	0.77	0.452
48	510.0	10.63	0.472	438	0.859	0.474	103	0.20	0.48	396	0.78	0.472
50	520.5	10.41	0.492	456.5	0.877	0.494	113	0.22	0.5	402	0.77	0.492
52	530.5	10.20	0.512	475	0.895	0.514	120	0.23	0.52	410	0.77	0.512
54	539.5	9.99	0.532	493	0.914	0.534	128	0.24	0.54	419	0.78	0.532
56	550.0	9.82	0.552	511	0.929	0.554	137	0.25	0.56	426	0.77	0.552
58	559.0	9.64	0.572	529.5	0.947	0.574	144.5	0.26	0.58	434	0.78	0.572
60	568.0	9.47	0.592	546	0.961	0.594	151.8	0.27	0.6	440.2	0.78	0.592
62	575.2	9.28	0.612	562	0.977	0.614	156.7	0.27	0.62	446	0.78	0.612
64	582.0	9.09	0.632	580	0.997	0.634	166.5	0.29	0.64	452	0.78	0.632
66	605.0	9.17	0.652	608	1.005	0.654	172.3	0.28	0.66	465	0.77	0.652
68	621.0	9.13	0.672	642	1.034	0.674	180	0.29	0.68	467	0.75	0.672
70	650.0	9.29	0.692	665	1.023	0.694	185.8	0.29	0.7	474	0.73	0.692
72	750.0	10.42	0.712	694	0.925	0.713	191.5	0.26	0.72	536	0.71	0.712
74	794.0	10.73	0.734	728	0.917	0.733	199	0.25	0.74	559	0.70	0.734
76	816.0	10.74	0.754	750	0.919	0.753	204.5	0.25	0.76	574	0.70	0.754
78	837.0	10.73	0.774	782	0.934	0.773	210.2	0.25	0.78	589	0.70	0.774
80	853.0	10.66	0.794	799	0.937	0.793	216.2	0.25	0.8	600	0.70	0.794
82	866.0	10.56	0.814	847	0.978	0.813	222	0.26	0.82	610	0.70	0.814
84	878.0	10.45	0.834	860	0.979	0.833	227.7	0.26	0.84	642	0.73	0.834
86	888.0	10.33	0.854	873	0.983	0.853	233	0.26	0.86	654	0.74	0.854
88	897.5	10.20	0.874	907	1.011	0.873	238.8	0.27	0.88	673	0.75	0.874
90	909.0	10.10	0.894	933	1.026	0.892	244.3	0.27	0.9	683	0.75	0.894
92	915.6	9.95	0.914	964	1.053	0.912	249.7	0.27	0.92	693	0.76	0.914
94	922.0	9.81	0.934	1007	1.092	0.932	254.9	0.28	0.94	701	0.76	0.934
96	928.5	9.67	0.954	1060	1.142	0.952	259.7	0.28	0.96	708	0.76	0.954
98	936.3	9.55	0.974	1122	1.198	0.972	264.2	0.28	0.98	716	0.76	0.974
100	942.8	9.43	0.994	1188	1.260	0.992	269	0.29	1	724	0.77	0.994



Figure 19. Young's modulus vs number of blows and depth of test (borehole diameter = 65 mm).

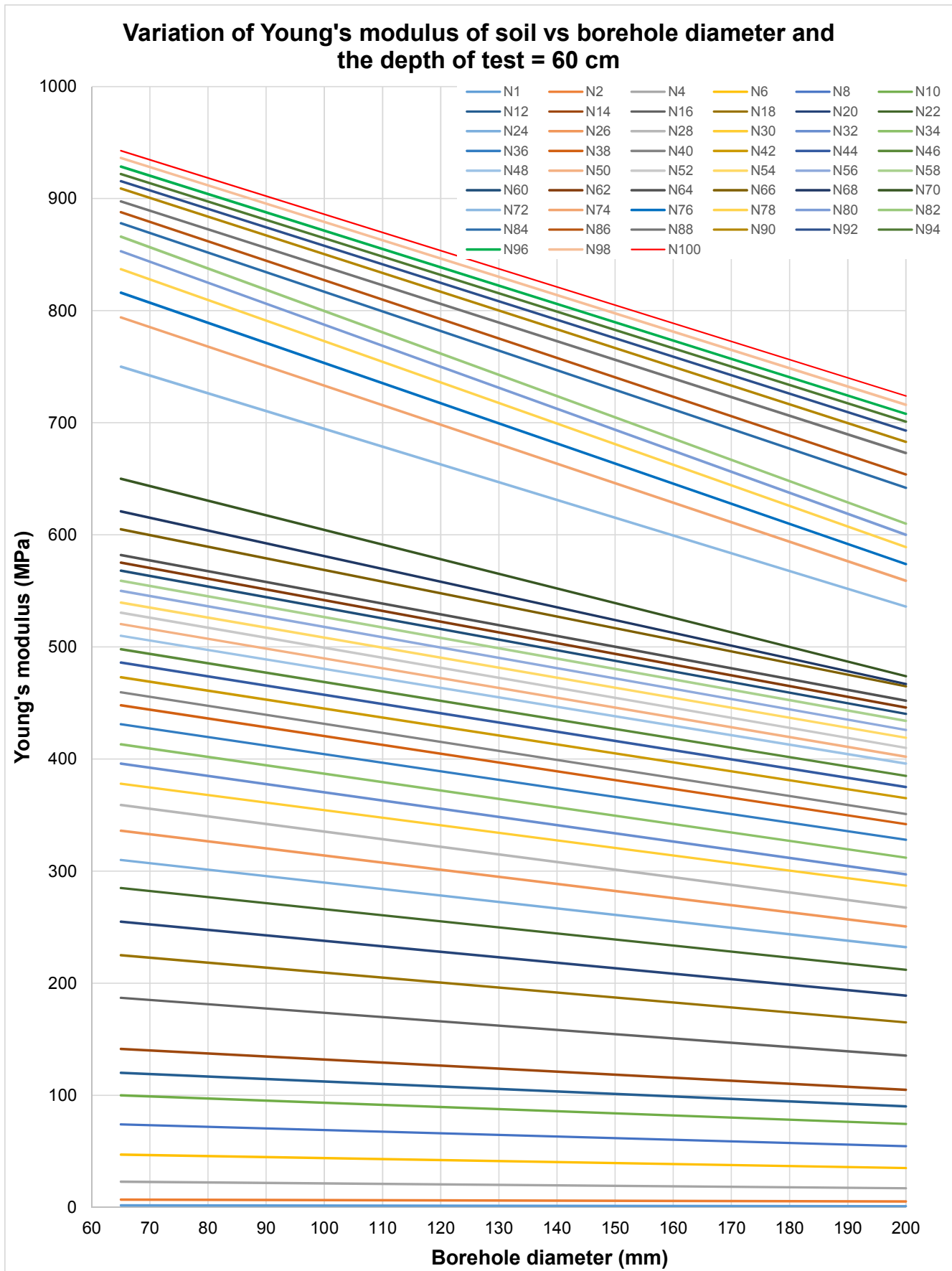


*Figure 20. Young's modulus vs number of blows and borehole diameter for depth=60 cm.*

## 6. Determination of the Young's Modulus of the Soil from $N_{SPT}$ by Interpolation of the Correction Factors

Table 5 below presents the summary of the 7 example cases treated with interpolation and double linear interpolation of the correction factors. The detailed calculation of the Young's modulus of case n°7 is carried out as follows:

The correction factor  $k_N$  is equal to

$$(9.13+9.29)/2=9.209$$

The correction factor  $k_D$  is equal to

$$(((1.034 - (13 - 5) \times (1.034 - 0.29) / (20 - 5)) + ((1.023 - (13 - 5) \times (1.023 - 0.29) / (20 - 5)))) / 2 = 0.63346$$

The correction factor  $k_B$  is equal to

$$(((1 - (120 - 65) \times (1 - 0.75) / (200 - 65)) + ((1 - (120 - 65) \times (1 - 0.73) / (200 - 65)))) / 2 = 0.8943$$

$$E = 69 \times 9.209 \times 0.63346 \times 0.8943 = 359.98$$

The value of this modulus can be read directly on the Table 4, by dividing by the  $k_D$  factor.

**Table 5.** Example of Young's modulus calculation with correction parameters  $k_N$ ,  $k_D$  and  $k_B$ .

Cas n°	$N_{SPT}$	D (m)	B (mm)	$k_N$	$k_D$	$k_B$	E (MPa)
1	15	1	65	10.8901786	1	1	163.35
2	35	3	65	12.0596405	0.8345519	1	352.25
3	53	7	65	10.0963319	0.8148799	1	436.05
4	69	13	65	9.20903361	0.6334621	1	402.52
5	87	15	65	10.2622225	0.5084354	1	453.94
6	53	7	90	10.0963319	0.8148799	0.9582871	417.86
7	69	13	120	9.20903361	0.6334621	0.8943274	359.98
8	87	15	150	10.2622225	0.5084354	0.8382945	380.53

## 7. Conclusion and Recommendations

### 7.1. Conclusion

We modeled the SPT test taking into account the experimental protocol in the field and the typical loading signal for this type of test. More than 500 numerical simulations have been carried out using the Finite Element calculation code Cast3M [2] in 2-D axisymmetric. We abandoned 3-D modeling in favor of 2-D modeling, because this required having a super computer and given the number of elements in this model, the time for a single calculation was considerable. For all the calculations, the Poisson's ratio was taken as equal to 0.3 for the soil and a unit weight of all the soils set at 17 kN/m<sup>3</sup>. We have shown that the strains obtained in our models were in perfect agreement with the levels of strains recommended for the in situ tests presented in Figure 16. From these dynamic calculations at small time steps, carried out in a semi-infinite soil mass without water table, it appears that the Young's modulus of the soils determined by our method, strongly depends on the number of blows at the SPT of the test depth and the diameter of the borehole. Charts, Tables for practical use and a direct relationship for determining the Young's modulus of soils by this method have been established and proposed in the framework. From the results of this work, it is already obvious to obtain the Young's modulus of a soil profile

after a good field test. This modulus now makes it possible to calculate geotechnical structures in stress-strain in the field of linear elasticity and to be able to control the admissible settlements of soil structures.

### 7.2. Recommendations

More precise methods, such as numerical calculations, must be used when the soil-structure interaction has a dominant influence. Numerical methods have the ability to take into account macroscopic soil heterogeneities (layers with different characteristics or heterogeneity in plan); the same applies to the heterogeneity caused by different loading levels depending on the points of the soil mass, in the case of a soil with non-linear behavior. For the practical resolution of soil-foundation-structure interaction problems, and in particular the calculation of displacements of shallow and deep foundations, retained walls, numerical methods must be used. The results presented in this paper must be reliably used to feed the mechanical behavior models of the soils implemented in the numerical calculation codes of the structures when only the results of in situ tests of the SPT type are available. Currently, given the large number of numerical modeling carried out in projects, it is strongly recommended to evaluate the parameters of the models from the data of in situ tests which have the capacity to obtain the quantity sought in any type of soil (loose sands, saturated clays,...).

Soon, we will develop a method based on the determination of the Young's modulus of soils from the dynamic cone resistance ( $q_d$ ) of the dynamic cone penetrometer which is



intensively used in projects for the evaluation of the bearing capacity and settlement of foundations.

## References

- [1] Cast3M® (2020). Cast3M is a research FEM environment; its development is sponsored by the French Atomic Energy Commission, see web site: <http://www-cast3m.cea.fr/>.
- [2] Vesic (1961). Bending of beams resting on isotropic elastic solid. JSMFD, ASCE, vol. 87.
- [3] Gazetas G. (1991). Formulas and charts for impedances of surface and embedded foundations.
- [4] CFMS, (2011). Recommandations sur la conception, le calcul, l'exécution et le contrôle des fondations d'éoliennes, 113p.
- [5] Eskandari M, Shodja H, M, Ahmadi S, F, (2013). Lateral translation of an inextensible circular membrane embedded in a transversely isotropic half-space, *European Journal of Mechanics*, Vol. 1, pp. 134-143.
- [6] Ahmadi S, F, Eskandari M, (2014<sup>a</sup>) Rocking Rotation of a Rigid Disk Embedded in a Transversely Isotropic Half-Space. *Civil Engineering Infrastructures Journal*, Vol. 1, pp. 125-138.
- [7] Ahmadi S, F, Eskandari M. (2014<sup>b</sup>) Vibration Analysis of a Rigid Circular Disk Embedded in a Transversely Isotropic Solid. *Journal of Engineering Mechanics*, Vol. 140, pp. 1-13.
- [8] Zoa Ambassa, Amba J, C, (2018). A new Calculation Method for the Bearing Capacity of Shallow Foundations from the Shear Waves Velocity. *International Journal of Civil Engineering and Technology*, vol. 9 (5), pp. 83-94.
- [9] Amar S. Jézéquel J-F. (2000). Propriétés mécaniques des sols déterminées en place. *Technique de l'ingénieur; traité Construction*, document C 220-1, 25 p.
- [10] Youd T., L., Idriss I, M. (2001). Liquefaction Resistance of Soils: Summary Report from the 1996 NCEER and 1998 NCEER/NSF Workshops on Evaluation of Liquefaction Resistance of Soils. *Journal of Geotechnical and Geoenvironmental Engineering*, vol. 127, N°4, pp. 297-313.
- [11] Das, B. M. (2016). Principles of soil Dynamics, 3rd ed.; California State University: Sacramento, 2016.
- [12] Terzaghi K., Peck R, B, (1967). Soil Mechanics in Engineering Practice. 2<sup>nd</sup> edition John Wiley and Sons, 729 p.
- [13] Schmertmann J., H. (1975). Measurement of *in situ* Shear Strength, *Proceeding, Specialty Conference on in situ Measurement of Soil Properties*, ASCE, Vol. 96, N°. SM3, pp. 1011-1043.
- [14] Schmertmann J, H. (1978). Guidelines for Cone Penetration Test, Performance and design, U.S. Department of Transportation, report N°. FHWA-TS-78-209, Washington D.C.
- [15] Wolf T., F. (1989). Pile Capacity Prediction Using Parameter Functions, in *Predicted and Observed Axial Behavior of Piles, Results of a Pile prediction Symposium*, Sponsored by Geotechnical Engineering Division, ASCE, Evaston, III, June 1989, ASCE, Geotechnical Special Publication N°. 23, pp. 96-106.
- [16] Dikmen U. (2009). Statistical correlations of shear wave velocity and penetration resistance for soils, *Journal of Geophysics and Engineering*, vol. 6, pp. 61-72.
- [17] Hettiarachi H, Brown T. (2009). Use of the SPT blow counts to estimate shear strength properties of soils: energy balance approach, *Journal of Geotechnical and Geoenvironmental Engineering*, Vol. 135, pp. 830-834.
- [18] Bowles J, E. (1987). Elastic Foundation Settlement on Sand Deposits. *Journal of Geotechnical Engineering*, ASCE, Vol. 113, N°.8, pp. 846-860.
- [19] Kérisel J., Caquot A, (1956). Traité de mécanique des sols. Gauthiers-Villars éditeur, p. 129.
- [20] Combarieu O. (2006). L'usage des modules de déformation en géotechnique. *Revue Française de Géotechnique*, Vol. 114, p. 3-32.
- [21] Philipponnat G. Hubert G. (2002). *Fondations et ouvrages en terre*. Eyrolles, Paris, 548 p.
- [22] PLAXIS® (2018). Finite Element Code for Soil and Rock Analyses. Material Models Manual, v. 8, 218p.
- [23] Broutin M. (2010). Assessment of flexible airfield pavements using Heavy Weight Deflectometers, Doctor of Philosophy, ENPC, Paris, France, 370p.
- [24] Picoux B., EL Ayadi A., Petit C. (2009). Dynamic response of flexible pavement submitted by impulsive loading, *International Journal Soil Dynamics and Earthquake Engineering*, N°29, pp. 845-854.
- [25] DGAC-STBA-STAC. (2014). Auscultation des chaussées souples aéronautiques au HWD: Guide technique. *Service Technique de l'Aviation Civile française, février 2014*, 86p.
- [26] Zoa Ambassa, Amba J., C. (2017). Apport du FWD pour l'analyse dynamique et l'évaluation structurelle des chaussées souples. *Journal Afrique science*, vol. 13 (1), pp. 52-62.
- [27] Bouafia Ali (2018). Mécanique des sols. Problèmes résolus. OPU, P. 651.
- [28] Boussinesq J. (1885). Application des potentiels à l'étude de l'équilibre et du mouvement des solides Elastiques, Gauthiers-Villars, Paris.
- [29] Baguelin F, Jezequel J, F, Shields D, H. (1978). The presuremeter and foundation engineering. Trans Tech Publications, Clausthal, FRG, 617p.
- [30] Baud J. P., Gambin M. (2013). Détermination du coefficient rhéologique  $\alpha$  de Ménard dans le diagramme Pressiorama. Proceedings of the 18<sup>th</sup> International Conference on Soil Mechanics and Geotechnical Engineering, Paris 2013, pp. 487-490.
- [31] British Standards Institution (2012). Geotechnical investigation and testing – field testing. *Menard pressure meter test*. London, BSI. BS EN ISO 22476-4: 2012.
- [32] EN ISO 22476-1. (2013). Geotechnical investigation and testing- Field testing. Part 1: Electrical cone and piezocone penetration test.
- [33] Robertson, P. K. (2009). Interpretation of Cone Penetration Test-a unified approach. *Canadian Geotechnical Journal*, N°. 46, pp. 1337-1355.



- [34] Robertson, P. K., Cabal K. L. (2014). Guide to Cone Penetration Testing for Geotechnical Engineering. Gregg Drilling & Testing, Inc, USA, 6<sup>th</sup> edition, 133p.
- [35] Sanglerat G. (1972). The penetrometer and Soil Exploration, Elsevier Publishing Company, Amsterdam, 464 p.
- [36] Burland J, B, Burbidge M, C. (1985). Settlement of foundations on sand and gravel. *Proceedings ICE*.
- [37] Strout L. (1989). The Standard Penetration Test - Application and Interpretation.
- [38] Skempton A-W., MacDonald D-H. (1956). Allowable settlement of building. *Proc. Instn Civ. Engrs*, Part 3: 5, pp. 727-768.
- [39] Ricceri G., Soranzo M. (1985). An analysis of allowable settlements of structures. *Rivista Italiana di Geotechnica*, vol. 19, p. 177.
- [40] Sneddon Ian N. (1947). Boussinesq's problem for a rigid cone. The Department of Natural Philosophy, The University of Glasgow, pp. 492-507.
- [41] Fox E. N. (1948). The mean elastic settlement of a uniformly loaded area at a depth below the ground surface. *Proceedings, 2nd International Conference on Soil Mechanics and Foundation Engineering*, Rotterdam, vol. pp. 129-132.
- [42] Giroud J, P. (1972). Mécanique des sols. Tables pour le calcul des fondations. Tome 1 (Tassement), Dunod, 360 p.
- [43] Winterkorn H. F., Fang H. Y. (1975). Foundation Engineering Handbook, van Nostrand Reinhold Company.
- [44] PHRI-TSPHF (1980). Technical Standards for Port and Harbour Facilities in Japan: Bearing capacity of pile foundations, pp. 123-136.
- [45] Mayne P. W., Poulos Harry G. (1999). Approximate Displacement Influence Factors for Elastic Shallow Foundations. *Journal of Geotechnical and Geoenvironmental Engineering*, Vol. 125. N°6, June 1999, pp. 453-460.
- [46] Fellenius Bengt H. (2006). Basics of Foundation Design. Calgary, Alberta, Canada.
- [47] Sokolovskij V. V. 1960<sup>b</sup>. Statics of soil media. Translated from the second Russian edition (1954) by D. H. Jones and A. N. Schofield, Butterworths, London, 237 p.
- [48] Schmitt, P. (1995). Estimating the coefficient of subgrade reaction for diaphragm wall and sheet pile wall design, in French. *Revue Française de Géotechnique*, N° 71, 2<sup>e</sup> trimestre 1995, pp. 3-10.
- [49] AFNOR EC7 (2014). Calcul géotechnique - Ouvrages de soutènement - Ecrans, norme NF P 282.